Spatiotemporal Modulation of Light in Microscale Selective Laser Sintering for Enhanced Process Resolution

Aaron Liao[1], Joshua Grose[1], Heejin Kim[2], Michael Cullinan[1], Chinedum Okwudire[2]

[1]Department of Mechanical Engineering
The University of Texas Austin
Austin, TX, USA

[2]Department of Mechanical Engineering
University of Michigan
Ann Arbor, MI, USA

INTRODUCTION

Many traditional metal additive manufacturing (AM) processes are increasingly applicable in industries such as aerospace, biomedical, and electronics due to their ability to handle intricate macroscale structures. However, the current commercially available AM tools have resolutions on the scale of hundreds of microns, which is too high for the required feature sizes in various microscale applications. As a result, there is a push towards the development of metal AM techniques that offer accuracies in the micron and sub-micron range [1]. The microscale selective laser sintering tool (μ-SLS), created at The University of Texas at Austin, aims to produce features smaller than 5 μm with high throughput, primarily targeting applications for high mix semiconductor packaging, and fine pitch metallization in advanced packaging [2].

The μ-SLS process starts by dispensing a bed of metal nanoparticles (NPs) on a substrate, followed by the translation of the NP bed under a sintering subsystem. This optical system consists of a 808 nm quasi-continuous wave laser coupled to a digital micromirror device (DMD) which projects an image through a set of collimating and focusing lenses shown below.

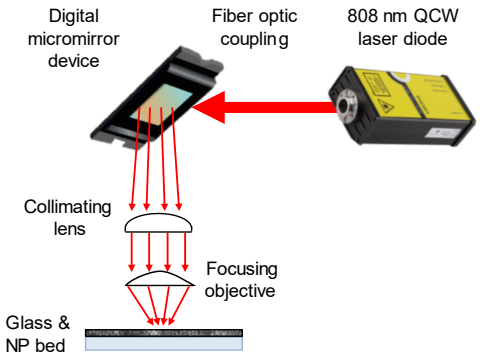

Figure 1: Schematic showing the optical system used for sintering in μ-SLS.

The DMD consists of a 1920 x 1080 array of micromirrors which can be directed to reflect an incident beam towards the substrate (on) or away to a heatsink (off). Each mirror on the DMD is demagnified to 1.2 x 1.2 μm. The resulting DMD surface projected onto the NP bed spans approximately 2.3 x 1.3 mm. Each individual mirror can be switched on or off at 9.5 kHz for 1-bit binary patterns. They can also be temporally modulated to express effective grayscale patterns at up to 8-bit resolution. This capability has not yet been fully utilized in the current prototype μ-SLS tool, but it can be used to control thermal gradients within the particle bed. The goal of this work is to harness this ability through both passive and active correction methods. The passive approach focuses on improving uniformity across the entire exposure region, while the active approach leverages an existing control framework to reduce the error between fabricated and expected feature sizes to less than 5% across the exposure area.

OPTICAL FIELD INTENSITY CORRECTION

Optical defects and intensity nonuniformity can be corrected using spatial light modulators. DMD light modulation techniques have been employed to enhance uniformity and process resolution in numerous lithography/DLP applications through measuring nonuniformity with a beam profiler [3]. Previous methodology for generating field correction directly correlated diameters of sintered features across the frame to the magnitude of intensity instead of using beam profiler measurements [4].

In this work, an Ophir SP928 beam profiler was placed at the plane of focus to measure the projected intensity that the substrate experiences during sintering. A static field correction was generated and applied to all masks to compensate for the inherent spatial intensity nonuniformity of the optical system and DMD.

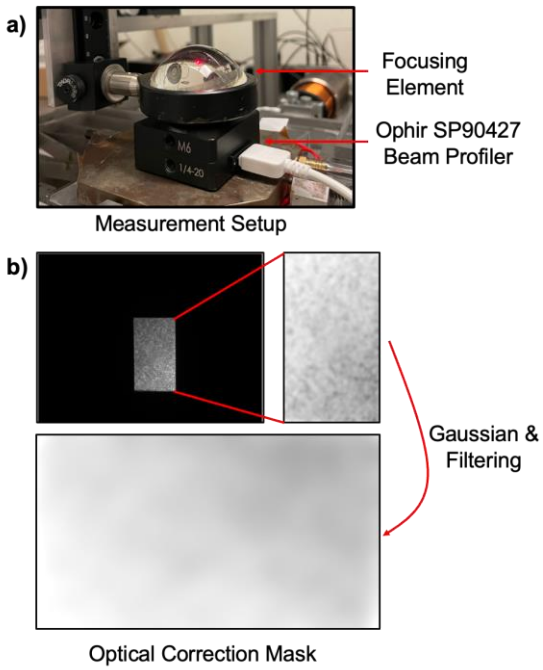

Figure 2: a) Beam Profiler measurement setup. b) Image acquired, filtered, and inverted to create final correction mask

After acquiring the beam profile image, it was filtered, and the intensity was inverted and normalized to the maximum value. This adjustment ensures that areas with lower initial intensity now receive more light to compensate. The increase in light is proportional to the overall intensity distribution, achieving a more uniform exposure across the entire region.

THERMAL GRADIENT COMPENSATION

Given that heat spreads laterally through the particle bed by means of conduction, areas with higher density of laser exposure will reach higher temperatures compared to regions at the edge of the frame where heat can conduct outwards to unexposed regions. Additionally, material changes within the particle bed as sintering progresses can make compensating for these effects more difficult. The custom FEA thermal modeling framework developed for nanoparticle sintering was employed to predict the temperature profile within a 2.3 x 1.3 mm rectangular region [5].

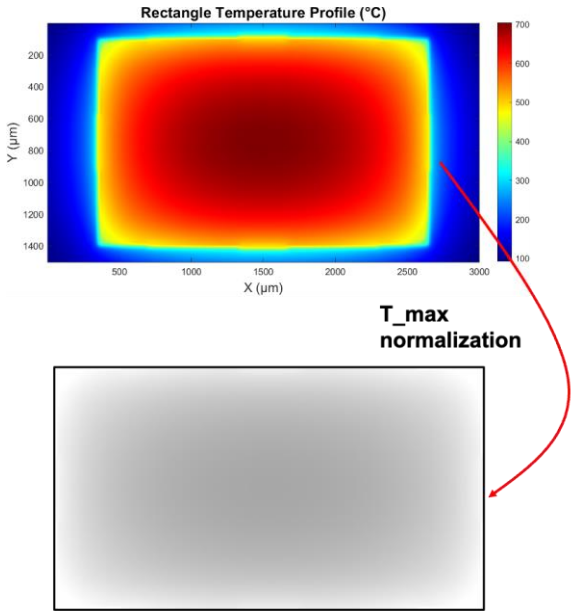

Figure 3: Temperature profile from thermal finite element simulation across a 2.3 x 1.3 mm area. Normalization using the max temperature and inversion were used to produce a correction mask.

The profile was normalized by the highest temperature value, transforming it into a greyscale image. The complement of this image was then used to create an optical compensation mask for the DMD, using modulation of the laser power to counteract the natural rise in the thermal gradient.

PASSIVE INTENSITY CORRECTION

By combining the optical and thermal masks generated in the previous sections with a symmetric mask, we can evaluate the effectiveness of this approach in improving thermal uniformity across the entire 2.3 x 1.3 mm exposure frame. The DMD accepts 1920 x 1080 bitmap images with values between 0 and 1. Once the desired pattern is selected, the correction masks are composited with the image through an element-wise multiplication operation to form the final exposure mask.

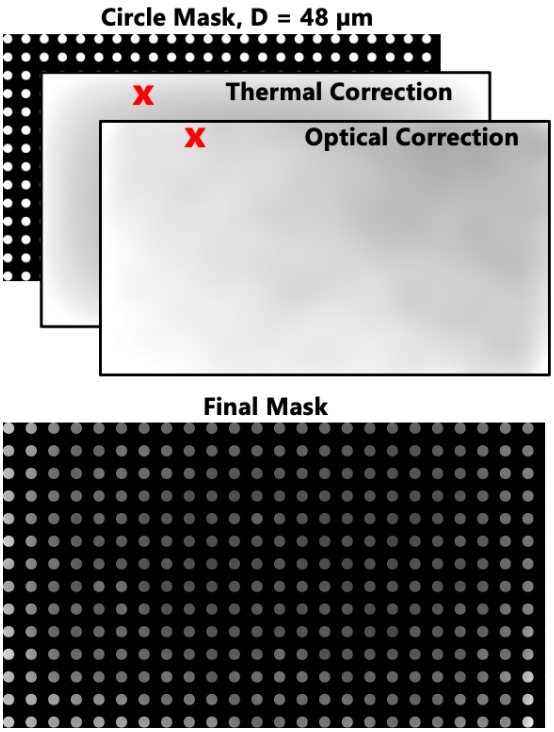

Figure 4: Element-wise multiplication operation for 50 µm diameter circle mask, resulting in final mask correcting for thermal and optical gradients.

The selected mask is a 14 x 24 array of dots, each with a 50 µm diameter. This pattern was chosen for its symmetry, allowing the gradient of final part diameters across the frame to directly reflect the temperature gradient experienced during laser exposure.

To analyze the effects of the modulation approach, 5 samples were created for both the modulated and unmodulated masks. Solvent was used to wash away unsintered nanoparticles surrounding the parts from each sample before imaging. The laser power for the modulated and unmodulated cases was 4.31 W and 2.85 W, respectively, with the laser activated for 2.5 seconds. The power discrepancy between the two cases was necessary to maintain the same average power input across all samples, as the modulation approach reduces the average intensity of the target mask. Microscope images were taken of the samples, and the Hough circle transform algorithm was used to automatically measure the diameters of the circles in the images. The following figure displays the diameters of the circles across the frame for both the modulated and unmodulated masks.

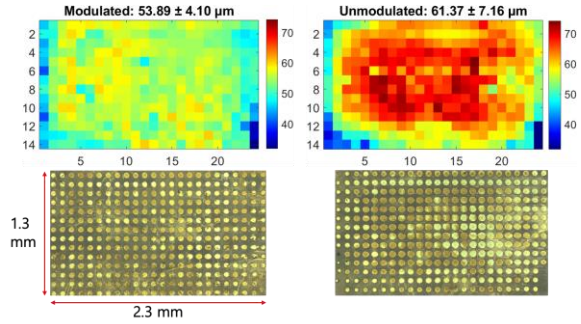

Figure 5: Heat maps comparing the size uniformity of circles produced by modulated and unmodulated masks. The average circle diameter produced at the position within the exposure frame is shown for both cases (n = 5).

The average diameter of the circles in the unmodulated case is 61.37 ± 7.16 µm, compared to 53.89 ± 4.10 µm for the corrected case. In the unmodulated case, the circles near the center of the frame are significantly larger than those at the edges, with diameters up to 3.2 times greater than the smallest circles at the edges. Assuming the diameter distribution follows a Gaussian profile, centered physically at the middle of the exposure frame, the corrected approach has successfully reduced the thermal gradient across the frame by approximately 43%. A histogram showing the distribution of all circles created across the 10 samples is presented below.

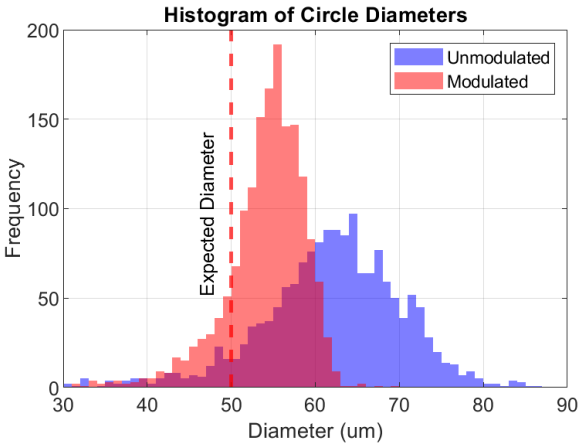

Figure 6: Histogram showing the distribution of circle diameters for both unmodulated and modulated cases, blue and red, respectively.

ACTIVE CORRECTION APPROACH

In this system, each white pixel in the mask represents a laser beam which individually heats a spot in the powder bed where the light is absorbed. The heat experienced by any point within the laser exposure area is proportional to the number of surrounding heat sources due to conduction through the adjacent particles. Pixels located near the center, with more neighbors, receive more heat due to higher pixel density, whereas those closer to the edges, with fewer neighboring pixels, experience less heat. This distribution creates a natural gradient of heat concentration from the center toward the edges. A finite difference heat transfer model was developed to predict temperature profile evolution. This model provided simplification and linearization to the previously mentioned custom finite element model designed to accommodate for changes in heat transfer properties in sintering of microscale metal powder.

A controller based on a quadratic optimization framework was developed to optimize laser power for each pixel, ensuring that sintering temperatures remain within the desired part boundaries while minimizing heat transfer to surrounding areas, which could lead to undesired part formation. This controller generates a series of masks that maintain sintering temperatures within the intended mask shape while keeping regions outside close to ambient temperatures. Detailed information about the construction of the finite difference model and the controller can be found in the reference paper [6].

While this work was initially demonstrated with a simple square with a coarse mesh with a 30 μm element size to ease computation, the goal is to extend this work to smaller and more difficult shapes which undergo more complex, and less intuitive thermal profiles during laser heating. The finite difference simulation was adjusted to use a finer mesh of 16 μm, and a semicircle with 1 mm diameter was selected as the target geometry due to its varying pixel density. Inside the semicircle, the pixel density is relatively uniform in the center, resulting in a higher concentration of heat. However, near the curved boundary and especially at the sharp corners of the flat edge, the pixel density drops, resulting in less heat accumulation in these areas. The finite difference model simulated temperature and optimized a mask sequence for a 3s laser exposure with a 0.2 second time step for a total of 14 masks. The pattern was projected onto a 0.5 μm thick copper nanoparticle bed, which was formed by spin-coating Novacentrix (Austin, TX) CI-005 ink onto a glass slide and fully dried. The static mask of the desired 1 mm diameter semicircle was also projected for 3s onto the same sample. Micrographs were captured and analyzed as shown in the figure below.

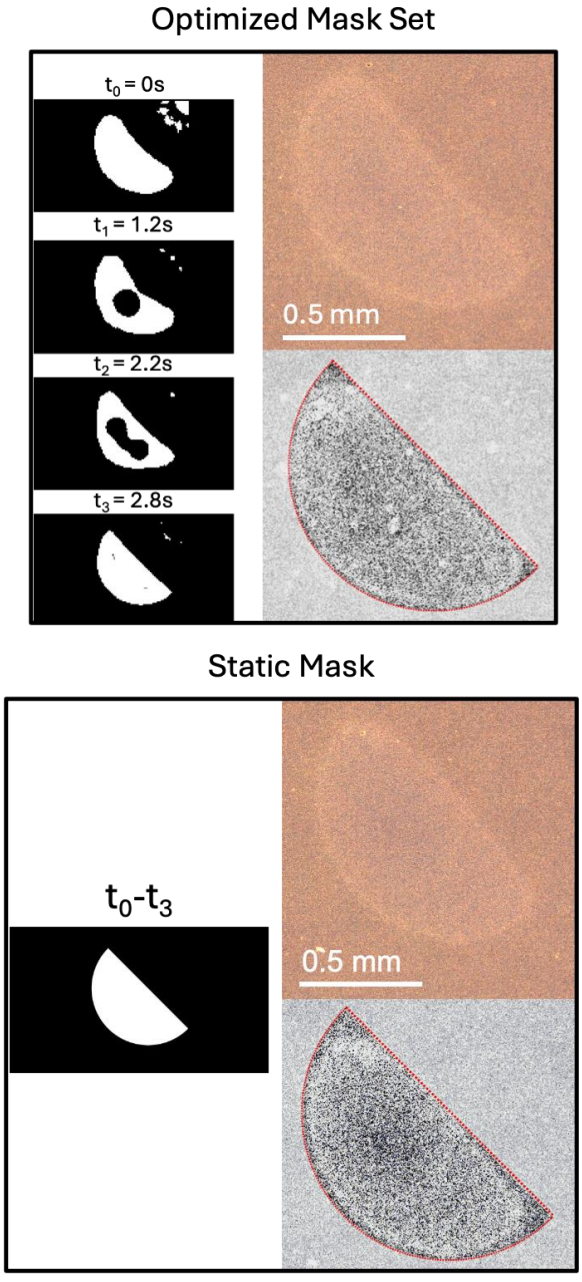

Figure 7: Micrographs showing comparison between the part boundaries of optimized and static masks. Greyscale and contrast filters were applied, and desired geometric outline was overlaid. Mask evolution is shown to the left of each respective set of micrographs.

In the figure above, the part error is visually represented by the black pixels adjacent to the red boundary overlaid the filtered micrograph. The static mask is capable of filling 92% of the desired part boundary, while the optimized mask set improves this, achieving a 97% fill of the target area. The difference at the boundary is most pronounced at the sharp edges of the semicircle, where a static mask of the desired shape fails to deliver sufficient heat to initiate part formation. The optimized mask sequence, however, improved performance in these corners by allowing the controller to add pixels outside the intended boundary—an adjustment that is not intuitive to do manually.

This geometry provided a useful test case to prove the effectiveness of the controller, as in the static mask case, the semicircle's shape inherently generates a gradient, with higher heat concentrated centrally and lower heat at the edges and corners. The controller was able to succesfully correct for both of these gradients which inherently rise from conduction.

CONCLUSIONS

This work aimed to leverage the spatiotemporal modulation capabilities of the digital micromirror device in the μ-SLS optical system to improve spatial uniformity and resolution of fabricated parts. This was achieved through various methods of predicting and compensating for temperature gradients caused by thermal conduction and optical defects, using both passive and active intensity modulation approaches.

Passive correction involved optical field measurements and thermal predictions to create compensation masks to reduce the thermal gradient across the projection area. These optical corrections can be broadly applied to future masks, whether for passive or active modulation, that require full-frame exposure. Although this specific approach may not apply directly to less symmetric shapes, the combination of modeling efforts and controller design can be combined with the optical correction to manage thermal gradients.

For further improvements on the active modulation approach, enhancing the accuracy of the finite difference model will be essential to provide the controller with more reliable temperature data. However, as finer meshes are required for more complex shapes, the finite difference method becomes computationally expensive at larger array sizes. To address this, alternative models may be needed, such as linearizing a surrogate model based on the finite element approach, which offers significantly more accurate temperature predictions. This approach could strike a balance between computational efficiency and the higher resolution needed for more intricate geometries. Additionally, testing a wider range of mask sets, particularly with more challenging geometries, will be critical for refining the constraints of the quadratic optimization problem used to generate these masks.

REFERENCES

[1] L. Hirt, A. Reiser, R. Spolenak, and T. Zambelli, "Additive Manufacturing of Metal Structures at the Micrometer Scale," *Adv. Mater.*, vol. 29, no. 17, 2017.

[2] Roy, N.K., Behera, D., Dibua, O.G. et al. "A novel microscale selective laser sintering (μ-SLS) process for the fabrication of microelectronic parts." Microsyst Nanoeng 5, 64, 2019.

[3] J. Yoon, K. Kim, and W. Park, "Modulated grayscale UV pattern for uniform photopolymerization based on a digital micromirror device system," Appl. Phys. Lett., vol. 111, no. 3, p. 033505, 2017.

[4] D. Behera, A. Liao, and M. A. Cullinan, "Passive intensity modulation of a pattern for fabricating near-net shaped features in microscale metal additive manufacturing," Manufacturing Letters, vol. 35, pp. 63–67, 2023.

[5] J. Grose, A. Liao, C. Foong, and M. A. Cullinan, "Part-Scale Simulation of Heat Affected Zone Development and Part Formation in a Microscale Metal Additive Manufacturing System," 2024.

[6] H. Kim, J. Grose, A. Liao, C, Okwudire, M. Cullinan, "A Model-based Control Framework for Microscale Selective Laser Sintering," presented at ASPE 2022 Annual Meeting , Bellevue, WA, USA, pp 18-23, 2022.